





Valence transition of the intermetallic compound $\text{Ce}_2\text{Rh}_2\text{Ga}$ probed by resonant x-ray emission spectroscopy

Hitoshi Sato ^{1,*}, Takuma Matsumoto,² Naomi Kawamura ³, Kazuhiro Maeda,² Toshiro Takabatake ⁴, and André M. Strydom ^{5,6}

¹Hiroshima Synchrotron Radiation Center, Hiroshima University, Higashi-Hiroshima 739-0046, Japan


²Graduate School of Science, Hiroshima University, Higashi-Hiroshima 739-8526, Japan

³Japan Synchrotron Radiation Institute (JASRI), Sayo, Hyogo 679-5198, Japan

⁴Department of Quantum Matter, Graduate School of Advanced Science and Engineering, Hiroshima University, Higashi-Hiroshima 739-8530, Japan

⁵Highly Correlated Matter Research Group, Physics Department, University of Johannesburg, PO Box 524, Auckland Park 2006, South Africa

⁶Max Planck Institute for Chemical Physics of Solids, 40 Nöthnitzerstr. D-01187 Dresden, Germany

 (Received 8 October 2021; revised 10 December 2021; accepted 16 December 2021; published 10 January 2022)

We have investigated the Ce valence of an intermetallic compound $\text{Ce}_2\text{Rh}_2\text{Ga}$ with a phase transition at $T_i = 128.5$ K by means of high-energy resolution fluorescence-detected x-ray absorption spectroscopy (HERFD-XAS) and resonant x-ray emission spectroscopy (RXES) around the Ce L_3 edge. The HERFD-XAS spectra in the whole temperature range from 300 to 3 K exhibit weak f^0 (Ce^{4+}) and f^2 (Ce^{2+}) peaks as well as the f^1 (Ce^{3+}) main peak, indicating that the Ce $4f$ electrons hybridize with the conduction electrons. With decreasing temperature from 125 to 100 K across T_i , the f^1 peak is reduced, while the f^0 peak is enhanced. Concomitantly, the Ce $L\alpha_1$ RXES intensity taken at the f^2 peak of the HERFD-XAS spectrum decreases. These spectroscopic results indicate that the phase transition at T_i of $\text{Ce}_2\text{Rh}_2\text{Ga}$ is driven by a valence transition of the Ce ions.

DOI: [10.1103/PhysRevB.105.035113](https://doi.org/10.1103/PhysRevB.105.035113)

I. INTRODUCTION

Ce- and Yb-based intermetallic compounds show astonishing physical phenomena such as the Kondo effect, Ruderman-Kittel-Kasuya-Yosida (RKKY) interaction, heavy-fermion behavior, valence fluctuation, and so on, which are originated from the hybridization between the localized $4f$ electrons and conduction electrons [1]. The rare-earth ions in compounds are usually in the trivalent state, while the Ce and Yb valence states often fluctuate between Ce^{3+} and Ce^{4+} , and Yb^{3+} and Yb^{2+} , respectively. Furthermore, the valence transition is induced with changing temperature, pressure, magnetic field, and chemical composition [2].

Among such examples, the valence transition of a pure Ce metal has been well studied, which takes place with a first-order isostructural ($fcc \rightarrow fcc$) phase transition from the high-temperature or low-pressure γ phase to the low-temperature or high-pressure α phase [3–6]. The magnetic susceptibility $\chi(T)$ in the γ phase obeys the Curie-Weiss law, while is nearly temperature independent in the α phase [7]. The transition is described as a localization-delocalization phenomenon of the Ce $4f$ states. Two scenarios for the $4f$ delocalization, the Kondo volume collapse model [8,9] and the Mott-Hubbard model [10], are under debate as the origin of the transition. The valence transition under pressure was directly observed by means of the Ce $L\alpha_1$ ($3d_{5/2} - 2p_{3/2}$) resonant x-ray emission spectroscopy (RXES). The theoretical analysis based on the Anderson impurity model showed that

the Ce valences increase from $\nu = 3.03$ at 0.15 GPa in the γ phase to $\nu = 3.19$ at 2 GPa in the α phase [4].

In comparison with the Ce metal, the valence transition of YbInCu_4 at $T_v = 42$ K (ambient pressure) has also been well studied [2,11–14]. The hard x-ray photoemission spectroscopy for the Yb $3d$ core states at $h\nu \sim 6$ keV revealed that the Yb valence decreases from 2.90 at high temperatures to 2.74 at low temperatures [15]. The Curie-Weiss type $\chi(T)$ sharply drops at T_v and becomes nearly constant at $T \leq T_v$. A structural modification from a cubic ($F\bar{4}3m$) to a tetragonal structures ($I\bar{4}m2$) has been revealed by a precise structural investigation using high-energy x-ray diffraction with synchrotron radiation [16].

Recently, a new Ce-based intermetallic compound $\text{Ce}_2\text{Rh}_2\text{Ga}$, which is one of the R_2T_2X family (R : rare earth, T : transition metal, X : p -metal), was synthesized and its physical properties were reported by Nesterenko *et al.* [17]. $\text{Ce}_2\text{Rh}_2\text{Ga}$ has dimorphic forms depending on the thermal treatment. The as-cast sample and the sample annealed at 900 °C have the orthorhombic La_2Ni_3 -type structure, while the sample annealed at 700 °C has the monoclinic $\text{Pr}_2\text{Co}_2\text{Al}$ -($\text{Ca}_2\text{Ir}_2\text{Si}$ -) type one. Of the two forms, the orthorhombic $\text{Ce}_2\text{Rh}_2\text{Ga}$ exhibits a phase transition at $T_i = 128.5$ K. Between 400 and 200 K, $\chi(T)$ follows the Curie-Weiss law with the effective magnetic moment of $2.54 \mu_B/\text{Ce}$, corresponding to Ce^{3+} . The negative Weiss temperature of $\theta_p = -120$ K was attributed to the antiferromagnetic interaction between the Ce ions. At T_i , $\chi(T)$ sharply drops by about 20% of the maximum value and continues to decrease down to 80 K. The specific heat C_p is nearly constant at $\sim 130 \text{ J/mol}_{\text{fu}} \text{ K}$ between 300 and 130 K and exhibits a cusp at T_i reaching to $\sim 424 \text{ J/mol}_{\text{fu}} \text{ K}$. The Sommerfeld coefficient

*jinjin@hiroshima-u.ac.jp

is estimated to be $\gamma = 172.5 \text{ mJ/mol}_{\text{Ce}} \text{ K}$ from the data below 20 K using $\text{La}_2\text{Rh}_2\text{Ga}$ data as a phonon contribution. The authors mentioned that the anomalies in $\chi(T)$ and $C_p(T)$ at T_i bear the signature of antiferromagnetic order, but the transition temperature of $T_i = 128.5 \text{ K}$ is extraordinary high [17] in comparison with typical Néel temperatures of Ce-based antiferromagnets. Therefore, a structural phase transition was proposed as an alternative scenario. In fact, a small monoclinic distortion is detected at around T_i as well as the noticeable changes in the lattice parameters and cell volume.

To reveal the mechanism of the phase transition in orthorhombic $\text{Ce}_2\text{Rh}_2\text{Ga}$ (hereinafter referred to as $\text{Ce}_2\text{Rh}_2\text{Ga}$ without “orthorhombic”), the investigation on electronic states is indispensable. It is noteworthy that the temperature dependence of $\chi(T)$ and the cusp of C_p at T_i resemble those of YbInCu_4 [2]. These similarities suggest that the phase transition of $\text{Ce}_2\text{Rh}_2\text{Ga}$ is driven by the valence transition in the Ce ion. This idea strongly motivated us to investigate the Ce-derived electronic states of this compound. A signature of valence transition is also seen in the changes in the lattice parameters and cell volume at around T_i [17]. In this paper, we have examined the temperature dependence of the Ce valence of $\text{Ce}_2\text{Rh}_2\text{Ga}$ by means of high-energy resolution fluorescence-detected x-ray absorption spectroscopy (HERFD-XAS) and the Ce $L\alpha_1$ resonant x-ray emission spectroscopy (RXES) around the Ce L_3 edge. We successfully detected the remarkable increase in the Ce valence with decreasing temperature across T_i , clearly indicating the valence transition in $\text{Ce}_2\text{Rh}_2\text{Ga}$.

II. EXPERIMENTS

The Ce L_3 HERFD-XAS and Ce $L\alpha_1$ REXS for $\text{Ce}_2\text{Rh}_2\text{Ga}$ were carried out at undulator beamline BL39XU of SPring-8 [18]. Undulator beam is monochromatized using a Si220 double crystal monochromator and focused onto the sample with the beam size of $0.1(\text{vertical}) \times 0.3(\text{horizontal}) \text{ mm}^2$. The Ce $L\alpha_1$ REXS spectra were measured using five Ge331 spherically bent crystals and a two-dimensional pixel detector (PILATUS). The HERFD-XAS spectra were collected by monitoring the intensity of the Ce $L\alpha_1$ fluorescence line with photon energy of $h\nu_{\text{out}} = 4840.2 \text{ eV}$, emitted after the Ce $2p_{3/2} - 5d$ absorption. The total energy resolution was about 0.6 eV. The temperature of the sample was controlled using a closed-circuit He cryostat and a heater attached to the sample holder. For the HERFD-XAS and REXS measurements, we used pieces cut from a single-crystalline $\text{Ce}_2\text{Rh}_2\text{Ga}$ sample, grown by the Czochralski method with a radio-frequency heating furnace. The sample was characterized by x-ray powder diffraction and the magnetic susceptibility measurements. The crystalline orientation relative to the polarization direction of the incident light was fixed throughout the experiments. The orientation dependence was not measured [19].

III. RESULTS

Figure 1(a) shows a temperature dependence of the Ce L_3 HERFD-XAS spectra of $\text{Ce}_2\text{Rh}_2\text{Ga}$ measured between 300 and 3 K as a function of incident photon energy ($h\nu_{\text{in}}$). The

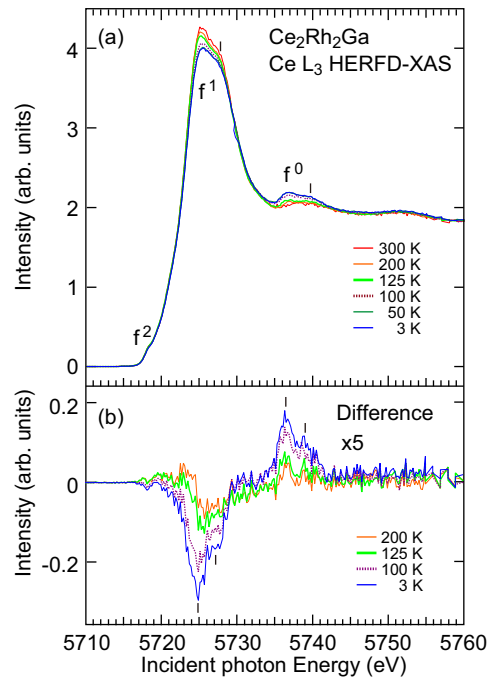


FIG. 1. (a) Temperature dependence of Ce L_3 HERFD-XAS spectra of $\text{Ce}_2\text{Rh}_2\text{Ga}$ measured between 300 and 3 K. Shoulder structures are observed in the f^1 and f^0 components as shown by vertical bars. (b) Difference spectra at 200, 125, 100, and 3 K obtained by subtracting the HERFD-XAS spectrum at 300 K. Two structures are noticed in the f^1 and f^0 components as shown by vertical bars.

spectra have been normalized with the total intensity in the measured region of $h\nu_{\text{in}} = 5700 \sim 5820 \text{ eV}$. The spectra exhibit a main peak at 5726 eV, so called white line, ascribed to the f^1 (Ce^{3+}) state [20]. On the other hand, a satellite feature at 5737 eV is attributed to the f^0 (Ce^{4+}) state. Both in the f^1 and f^0 peaks, shoulder structures are observed as shown by vertical bars in the figure. Since the absorption is caused by the $2p_{3/2} - 5d$ transition, the f^1 and f^0 features reflect the feature of the Ce $5d$ density of states (DOS). Such two components are also observed in the Ce L_3 HERFD-XAS spectra for $\text{Ce}(\text{Ru}_{1-x}\text{Fe}_x)_2\text{Al}_{10}$ due to band effects [21]. Coexistence of the f^1 and f^0 components indicates a presence of the hybridization between the Ce $4f$ electrons and conduction electrons ($c - f$ hybridization) in the whole temperature region, whereas the well localized $4f$ state of Ce^{3+} was indicated above T_i from the effective moment of $\chi(T)$. We also find a weak shoulder at 5718 eV, which is originated from the f^2 (Ce^{2+}) state [3,22]. A broad structure around 5752 eV is a part of the oscillations due to an extended x-ray absorption fine structure (EXAFS).

The fundamental features of the spectra remain unchanged with temperature, while the f^1 (f^0) peak is reduced (enhanced) gradually on cooling, indicating that the Ce valence shifts towards tetravalent. On the other hand, it is difficult to see clear variation of the f^2 shoulder because of the substantially weak intensity. Figure 1(b) shows a temperature dependence of the difference spectra obtained by subtracting the spectrum at 300 K. On cooling a negative structure at 5725 eV develops, corresponding to the reduction of the f^1

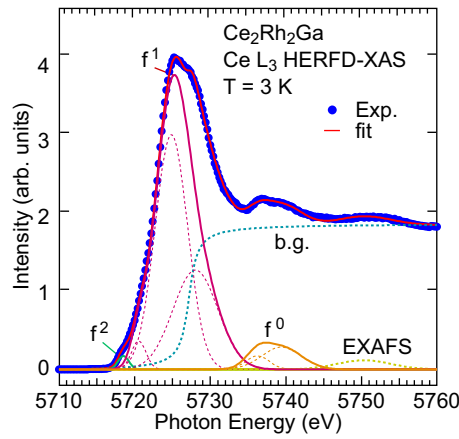


FIG. 2. Deconvolution of Ce L_3 HERFD-XAS spectrum of $\text{Ce}_2\text{Rh}_2\text{Ga}$ measured at 3 K into the f^0 , f^1 , and f^2 components with the contributions from the absorption edge and EXAFS structure.

structure. On the contrary, the f^0 enhancement is manifested in the positive structure at 5736 eV. Obviously, we find two components in the respective structures, reflecting the Ce $5d$ DOS feature. Note that the noticeable change is detected between 125 and 100 K, indicating that the temperature dependence of the HERFD-XAS spectra is related to the phase transition at T_i . We notice a small negative peak at 5718 eV in the difference spectra at 100 and 3 K, indicating that the f^2 shoulder is slightly reduced.

The relative intensities among the f^0 , f^1 , and f^2 components in the HERFD-XAS spectra provide the average number of the Ce $4f$ electrons, that is, the Ce valence v . In the ground state, v is roughly estimated from $v = 3 + (I_0 - I_2)/(I_0 + I_1 + I_2)$ with disregarding the final state interaction [20,22]. Here, I_0 , I_1 , and I_2 denote the intensities of the f^0 , f^1 , and f^2 components, respectively [19]. To deduce I_0 , I_1 , and I_2 , we deconvoluted the HERFD-XAS spectra by fitting with the conventional method [20]. As an example, a fit to the spectrum at 3 K is shown in Fig. 2. The f^1 feature was assumed to be expressed by three Gaussian functions as shown by dashed lines. In the fits of all spectra, we fixed the relative intensities, energy differences, and full widths at half maxima of the three Gaussian functions. Similarly, the f^0 feature was assumed to be expressed by two Gaussian functions, and the f^2 feature by one Gaussian function. A part of the EXAFS oscillation was also assumed by the Gaussian function. The intensity ratio between the f^1 and f^2 components was fixed for all temperatures by taking account of the RXES results as shown later. The edge jump due to the Ce^{3+} (f^1) L_3 absorption to continuum states was approximated by an arctangent function. The Ce^{4+} (f^0) and Ce^{2+} (f^2) L_3 absorptions were neglected, because of small contribution to the spectra. Using these curves, the spectra are well fitted as shown in Fig. 2.

Figure 3(a) shows the temperature dependence of the f^0 , f^1 , and f^2 intensities derived from the fits. With decreasing temperature from 300 K, the f^1 intensity gradually decreases until it drops across T_i while the f^0 intensity shows an opposite variation. The f^2 intensity, which was fixed so as to be proportional to the f^1 intensity, is almost independent of temperature on the scale of the vertical axis in Fig. 3(a). The

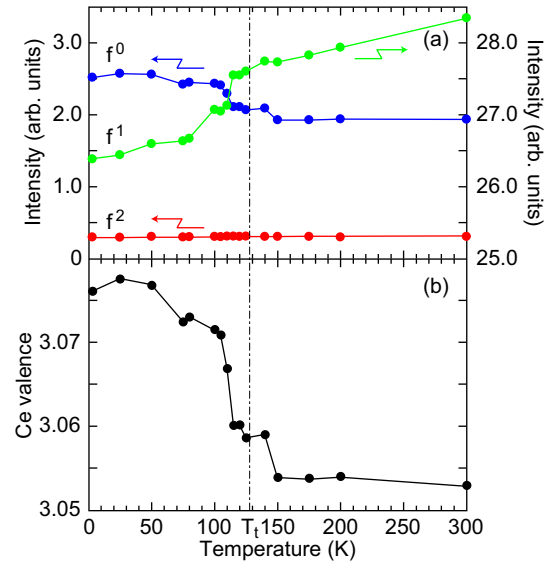


FIG. 3. (a) Temperature dependences of f^0 , f^1 , and f^2 intensities of HERFD-XAS spectra of $\text{Ce}_2\text{Rh}_2\text{Ga}$ obtained from the fits. (b) Temperature dependence of the Ce valences of $\text{Ce}_2\text{Rh}_2\text{Ga}$ deduced from the f^0 , f^1 , and f^2 intensities in (a).

Ce valences deduced from the f^0 , f^1 , and f^2 intensities are plotted as a function of temperature in Fig. 3(b). The Ce valence at 300 K is estimated to be $v \sim 3.053$ and almost constant down to 150 K. Between 125 and 100 K, the Ce valence remarkably increases to $v \sim 3.071$ and gradually to a little below $v \sim 3.08$ at $T \leq 50$ K.

To better assess the temperature dependence of the f^2 weight, we have measured the Ce $L\alpha_1$ RXES spectra. Figure 4(b) presents a series of the RXES spectra measured at 300 K with changing $h\nu_{\text{in}}$ from 5715 to 5760 eV around the Ce L_3 absorption edge. Energy transfer for the horizontal axis of the spectra is defined as the energy difference between the incident and emitted photon energies; $\Delta h\nu = h\nu_{\text{in}} - h\nu_{\text{out}}$. The vertical offset of each spectrum is scaled to $h\nu_{\text{in}}$ axis of the HERFD-XAS spectrum presented in Fig. 4(a). The feature of the RXES spectra in Fig. 4(b) strongly depends on $h\nu_{\text{in}}$. The spectrum at $h\nu_{\text{in}} = 5715$ eV, below the Ce L_3 absorption edge, already has weak intensity and exhibit a broad structure with a maximum at $\Delta h\nu = 885$ eV. With increasing $h\nu_{\text{in}}$ from 5715 to 5719 eV, the broad structure is gradually enhanced with no energy shift and no change of the feature, indicating that the broad structure is ascribed to the Raman component. With further increasing $h\nu_{\text{in}}$, the intensity of the spectrum further increases with changing the feature and reaches a maximum around the HERFD-XAS main peak ($h\nu_{\text{in}} = 5725$ eV). Above the main peak, there are the Ce $L\alpha_1$ fluorescence lines, which move toward the higher energy transfer linearly with $h\nu_{\text{in}}$ because of the constant $h\nu_{\text{out}}$ of 4840.2 eV.

Figure 4(c) shows the temperature dependence of the RXES spectra measured at $h\nu_{\text{in}} = 5718$ eV, corresponding to the f^2 peak of the HERFD-XAS spectrum. The spectra have been normalized to the $h\nu_{\text{in}}$ intensity. We find some fine structures at $\Delta h\nu = 878.0$, 879.5, and 881.5 eV in addition to the main peak at 885 eV. We recall that in the Ce $L\alpha_1$

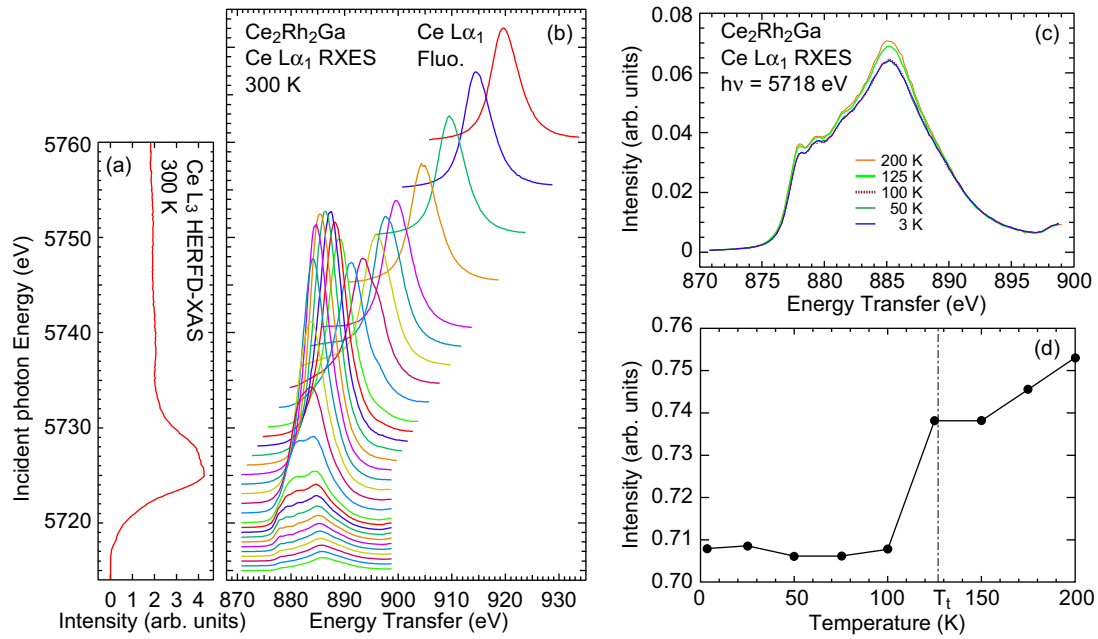


FIG. 4. (a) Ce L_3 HERFD-XAS spectrum of Ce₂Rh₂Ga measured at 300 K. (b) $h\nu_{\text{in}}$ dependence of Ce $L\alpha_1$ RXES spectra around the Ce L_3 absorption edge measured at 300 K. Horizontal axis is an energy transfer defined by $\Delta h\nu = h\nu_{\text{in}} - h\nu_{\text{out}}$. Vertical offset of each spectra has been scaled to $h\nu_{\text{in}}$ axis in the HERFD-XAS spectrum in (a). (c) Temperature dependence of RXES spectra taken at $h\nu_{\text{in}} = 5718$ eV, corresponding to the f^2 peak of the HERFD-XAS spectrum. (d) Temperature dependence of total intensities of RXES spectra at $h\nu_{\text{in}} = 5718$ eV in (c).

RXES spectrum measured around the f^2 HERFD-XAS peak, two structures due to the f^1 and f^2 components appear at the higher and lower energy transfer, respectively, with the energy distance of about 7 eV [4,20]. In particular, the f^2 component at the lower energy transfer is observed emphatically. In the series of the RXES spectra in Fig. 4(b), with increasing $h\nu_{\text{in}}$ from 5715 eV, the structures at $\Delta h\nu = 878.0$ and 879.5 eV seem to be slightly enhanced in comparison with those at $\Delta h\nu = 881.5$ and 885 eV at $h\nu_{\text{in}} = 5718$ eV. Thus, the former two structures are ascribed to the f^2 component, while the latter two structures to the f^1 component. In Fig. 4(c), we notice that the whole intensity steeply reduced on cooling from 125 to 100 K, again related to the phase transition at T_t . On the other hand, the overall spectral feature including the relative intensity hardly changes, which means that the f^2 weight relative to the f^1 weight is almost invariant across T_t . The total intensities of the RXES spectra are plotted as a function of temperature in Fig. 4(d). A similar behavior is also detected in the RXES spectra measured at $h\nu_{\text{in}} = 5719$ eV. These observations clearly show that the f^2 weight decreases with decreasing temperature across T_t with keeping the ratio with respect to the f^1 weight constant.

IV. DISCUSSION

We observed the remarkable increase in the Ce valence of Ce₂Rh₂Ga with decreasing temperature from 125 to 100 K. The temperature range is slightly below $T_t = 128.5$ K, where $\chi(T)$ sharply drops. This shift in temperature may be caused by heating of the sample due to high intense synchrotron radiation. We comment that the derived Ce valence is slightly underestimated as shown in Fig. 5 in comparison with the actual value in the ground state due to the final state effect

[22]. Nevertheless, the experimental results clearly reveal the valence transition across T_t .

The valence transition is consistent with the temperature-dependent lattice parameters, reported in the supplementary materials of Ref. [17] (Fig. S3 in that paper). On cooling from 150 to 80 K across T_t , the orthorhombic a and b axis parameters gradually contract, while the c axis parameter expands. As a whole, the unit cell volume decreases from $V \sim 423 \text{ \AA}^3$ at 150 K to $V \sim 413 \text{ \AA}^3$ at 80 K with the volume change of $\Delta V/V \sim 0.024$. A small monoclinic distortion is detected below T_t . The structural transition has not clearly been found and is under investigation at present. On the other hand, the present HERFD-XAS shows that the Ce valence increases from $v \sim 3.054$ at 150 K and ~ 3.073 at 80 K, providing $\Delta v/v \sim 0.0062$.

Let us compare these values of $\Delta V/V$ and $\Delta v/v$ with those of the valence transition in the Ce metal at the $\gamma - \alpha$ transition induced by applied pressure. The Ce valences of the Ce metal are estimated to be 3.03 at 0.15 GPa in the γ phase and 3.19 at 2 GPa in the α phase by means of Ce $L\alpha_1$ RXES [4], resulting in $\Delta v/v \sim 0.051$. By this transition, the lattice volume decreases from 34.2 \AA^3 at 0.15 GPa to 26.7 \AA^3 at 2 GPa with $\Delta V/V \sim 0.25$ [23]. Both values of $\Delta V/V$ and $\Delta v/v$ of Ce₂Rh₂Ga are smaller than those of the Ce metal by just about an order of magnitude. This means that the volume change relative to the valence change is comparable between the Ce metal and Ce₂Rh₂Ga. Note that the two systems have the difference in both the crystal structure and density of the Ce ion in the lattice.

Another example of the Ce-based compound showing a first-order valence transition is CeNi_{1-x}Co_xSn ($0.35 \leq x \leq 0.40$) with $T_v = 75 - 40$ K [24]. The $\chi(T)$ exhibits the Curie-Weiss behavior above T_v and sharply decreases at T_v , like in

$\text{Ce}_2\text{Rh}_2\text{Ga}$ [17]. In case of $\text{CeNi}_{1-x}\text{Co}_x\text{Sn}$ with $x = 0.38$, the unit cell volume abruptly decreases at 45 K with the volume change of $\Delta V/V \sim 0.003$. The Ce L_3 HERFD-XAS results were also reported for $x = 0.33$ (as-cast sample) and 0.38 [25]. For $x = 0.33$, the f^0 peak slightly increases relative to the f^1 peak on cooling [26]. Although the Ce valence was not estimated in Ref. [25], the valence change seems to be comparable with $\text{Ce}_2\text{Rh}_2\text{Ga}$ from the temperature-dependent HERFD-XAS spectra for $x = 0.33$. Thus, the ratio of the volume change relative to the valence change for $\text{Ce}_2\text{Rh}_2\text{Ga}$ is similar with those in the Ce metal and $\text{CeNi}_{1-x}\text{Co}_x\text{Sn}$. This fact suggests that the lattice contraction of $\text{Ce}_2\text{Rh}_2\text{Ga}$ is induced by the valence transition.

The transition temperature of 128.5 K for $\text{Ce}_2\text{Rh}_2\text{Ga}$ is substantially higher than 40 K ($x = 0.40$) and 75 K ($x = 0.35$) for $\text{CeNi}_{1-x}\text{Co}_x\text{Sn}$. In addition, the lattice parameters of $\text{Ce}_2\text{Rh}_2\text{Ga}$ change gradually at around T_t , in contrast to the sharp change of $\text{CeNi}_{1-x}\text{Co}_x\text{Sn}$. However, the sharp drop in $\chi(T)$, and amounts of the Ce valence and volume changes are comparable for both compounds. The phase transition in $\text{CeNi}_{1-x}\text{Co}_x\text{Sn}$ is interpreted by the first-order valence transition from the localized $4f$ state to the itinerant $4f$ state. For $\text{Ce}_2\text{Rh}_2\text{Ga}$, the increases of the Ce valence or the enhancement of the f^0 component in the Ce L_3 HERFD-XAS spectra below T_t indicate that the $c - f$ hybridization becomes stronger in the low temperature phase. In the same line with $\text{CeNi}_{1-x}\text{Co}_x\text{Sn}$, the phase transition of $\text{Ce}_2\text{Rh}_2\text{Ga}$ is described as follows. With decreasing temperature from about 150 K, the Ce valence starts to increase and the volume of the unit cell to decrease around 150 K. As the result, the $c - f$ hybridization is gradually enhanced with keeping the local Ce $4f$ moment unchanged down to T_t . At T_t , due to the remarkable increases of the $c - f$ hybridization and the Ce valence, the local moment is abruptly screened and the magnetic susceptibility suddenly drops. Below T_t , the Ce valence and cell volume continue to vary down to 80 K. At present, we are not able to derive the Kondo temperature T_K , which is a measure of the $c - f$ hybridization strength. Further studies by means of other microscopic tools are required to reveal the origin of the phase transition of $\text{Ce}_2\text{Rh}_2\text{Ga}$.

Finally, we estimated the Ce valences in the ground state by taking account of the final state effect. Thereby, we used the model proposed by Imer and Wuilloud [27], which is a simplified version of the Gunnarsson-Schönhammer model based on the single-impurity Anderson model [28,29]. According to their model, the Hamiltonian for the ground state H_g for the Ce compounds is given by

$$H_g = \begin{pmatrix} 0 & \Delta & 0 \\ \Delta & \varepsilon_f & \sqrt{2}\Delta \\ 0 & \sqrt{2}\Delta & 2\varepsilon_f + U_{ff} \end{pmatrix} \quad (1)$$

with the basis set of $|f^0\rangle$, $|f^1\rangle$, and $|f^2\rangle$, where ε_f and U_{ff} represent the energy of the $4f$ state and the Coulomb interaction energy between the $4f$ electrons, and Δ is defined by $\Delta = \langle f^1 | H_g | f^0 \rangle$. The diagonalization of H_g provides the ground state $|g\rangle = s_0|f^0\rangle + s_1|f^1\rangle + s_2|f^2\rangle$ with the lowest energy eigenvalue and the Ce valence in the ground state is given by $v = 4 - |s_1|^2 - 2|s_2|^2$. Similarly, the Hamiltonian

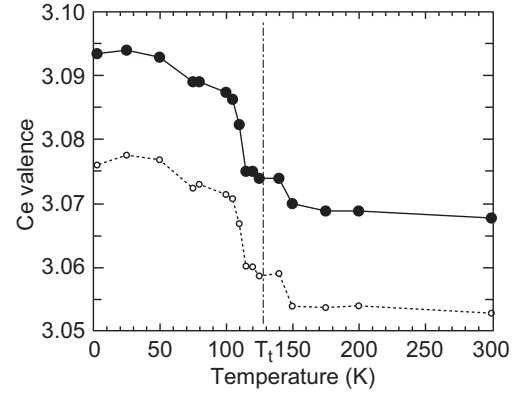


FIG. 5. Temperature dependence of the Ce valences in the ground state of $\text{Ce}_2\text{Rh}_2\text{Ga}$ obtained by taking account of the final state effect using the simple model [27] (solid circles). The Ce valences derived by neglecting the final state effect in Fig. 3(b) (open circles) are also shown for comparison.

for the Ce L_3 XAS final state H_f is given by

$$H_f = \begin{pmatrix} 0 & \Delta & 0 \\ \Delta & \varepsilon_f - U_{fc} + U_{fd} & \sqrt{2}\Delta \\ 0 & \sqrt{2}\Delta & 2(\varepsilon_f - U_{fc} + U_{fd}) + U_{ff} \end{pmatrix}, \quad (2)$$

where U_{fc} and U_{fd} are the $2p - 4f$ and $5d - 4f$ Coulomb interaction energies, respectively. The XAS intensity for the eigenstate of H_f , $|\tilde{f}^i\rangle = t_{i0}|f^0\rangle + t_{i1}|f^1\rangle + t_{i2}|f^2\rangle$ ($i = 0, 1, 2$), is obtained from $|s_0t_{i0} + s_1t_{i1} + s_2t_{i2}|^2$. Note that the XAS intensity for $|\tilde{f}^i\rangle$ corresponds to the experimental intensity of the f^i peak. We adjusted four parameters ε_f , Δ , U_{ff} , and $U_{fc} - U_{fd}$ so as to reproduce the relative intensities and relative centroid energies for the f^0 , f^1 , and f^2 components in the HERFD-XAS spectra. Derived parameters were $\varepsilon_f = -0.59$ eV, $U_{ff} = 5.28$ eV, and $U_{fc} - U_{fd} = 11.97$ eV. Only Δ values were changed with temperatures from 0.180 eV at 300 K to 0.226 eV at 3 K, which shows that the $c - f$ hybridization strength increases at low temperatures. As examples, the calculated XAS intensities at 300, 150, 80, and 3 K are summarized in Table I in comparison with those derived from the deconvolution of the HERFD-XAS spectra as in Fig. 2. The relative centroid energies of the f^1 and f^0 peaks to the f^2 peak are 7.3 and 20.2 eV in the experiments,

TABLE I. The calculated f^0 , f^1 , and f^2 XAS intensities ($I_{f_i}^{\text{calc.}}$) are compared with those derived from the deconvolution of the HERFD-XAS spectra ($I_{f_i}^{\text{exp.}}$) as in Fig. 2. Used Δ parameters are presented, while the other parameters are fixed to be $\varepsilon_f = -0.59$ eV, $U_{ff} = 5.28$ eV, and $U_{fc} - U_{fd} = 11.97$ eV.

| Temperature (K) | Δ (eV) | $I_{f^0}^{\text{calc.}}$ | $I_{f^0}^{\text{exp.}}$ | $I_{f^1}^{\text{calc.}}$ | $I_{f^1}^{\text{exp.}}$ | $I_{f^2}^{\text{calc.}}$ | $I_{f^2}^{\text{exp.}}$ |
|-----------------|---------------|--------------------------|-------------------------|--------------------------|-------------------------|--------------------------|-------------------------|
| 300 | 0.180 | 0.063 | 0.063 | 0.929 | 0.926 | 0.007 | 0.011 |
| 150 | 0.184 | 0.065 | 0.065 | 0.927 | 0.925 | 0.008 | 0.011 |
| 80 | 0.218 | 0.083 | 0.084 | 0.907 | 0.906 | 0.010 | 0.010 |
| 3 | 0.226 | 0.087 | 0.086 | 0.902 | 0.903 | 0.011 | 0.010 |

while the calculated values are 7.3 and 19.9 eV, respectively, for all temperatures. Figure 5 shows the deduced Ce valences in the ground state as a function of temperatures, which are larger than about 0.015 in comparison with those in Fig. 3(b). The valences of $v \sim 3.070$ at 150 K and $v \sim 3.089$ at 80 K results in $\Delta v/v \sim 0.0062$.

V. SUMMARY

To reveal the mechanism of the antiferromagnetic-like phase transition at $T_i = 128.5$ K in orthorhombic $\text{Ce}_2\text{Rh}_2\text{Ga}$ [17], we have investigated the Ce valence of this compound by means of the Ce L_3 HERFD-XAS and Ce $L\alpha_1$ RXES on a single crystal. The HERFD-XAS spectra between 300 and 3 K exhibit the small fraction of the f^0 component in addition to the f^1 main peak, indicating the weakly mixed valence state formed by the $c - f$ hybridization. The tiny f^2 shoulder is also detected below the f^1 main peak. With decreasing temperature from 300 K, the f^1 peak gradually decreases, while the f^0 peak increases. From the f^0 , f^1 , and f^2 intensities obtained by the fits to the HERFD-XAS spectra, the Ce valence at 300–150 K is evaluated to be $v \sim 3.053$. The Ce valence increases to $v \sim 3.073$ on cooling to 80 K across T_i and continues to increase to a little below $v \sim 3.08$ at 50 K (see also Fig. 5). In particular, the remarkable increase in the valence occurs between 125 and 100 K. The Ce $4f$ state in $\text{Ce}_2\text{Rh}_2\text{Ga}$ transforms from the rather localized state

in the higher temperature phase into the rather delocalized state in the low temperature phase. The valence transition is also observed as the decrease in the total intensities of the RXES spectra measured at $h\nu_{\text{in}} = 5718$ eV, corresponding to the f^2 component in the HERFD-XAS spectrum. The RXES results show the f^2 weight decreases on cooling across T_i with keeping the constant ratio to the f^1 weight. Thus, we conclude that the phase transition at T_i of $\text{Ce}_2\text{Rh}_2\text{Ga}$ is caused by the valence transition.

ACKNOWLEDGMENTS

The authors are grateful to H. Yamaoka for stimulating discussion and valuable comments to manuscript. They also thank Y. Tanaka for the support during the experiments. The experiments at BL39XU were performed under the approval of the Japan Synchrotron Radiation Research Institute (JASRI) (Proposals No. 2019B1359 and No. 2020A1322). The HERFD-XAS spectra were also measured at BL12XU under the approval of Taiwan Beamline (NSRRC Proposal No. 2019-3-033-1, SPring-8 Proposal No. 2019B4250). The authors thank H. Ishii and N. Hiraoka for the technical supports for the experiments at BL12XU. This work was financially supported by Grants-in-Aid from MEXT/JSPS KAKENHI Grant No. JP21K03473. A.M.S. thanks the SA-NRF (93549) and the URC/FRC of UJ for financial assistance.

-
- [1] H. v. Löhneysens, A. Rosch, M. Vojita, and P. Wölfle, Fermi-liquid instabilities at magnetic quantum phase transitions, *Rev. Mod. Phys.* **79**, 1015 (2007).
- [2] J. L. Sarrao, Physics of YbInCu_4 and related compounds, *Physica* **259-261**, 128 (1999), and references cited therein.
- [3] C. Dallera, M. Grioni, A. Palenzona, M. Taguchi, E. Anese, G. Ghiringhelli, A. Tagliaferri, N. B. Brookes, Th. Neisius, and L. Braicovich, $\alpha - \gamma$ transition in metallic Ce studied by resonant x-ray spectroscopies, *Phys. Rev. B* **70**, 085112 (2004).
- [4] J. P. Rueff, J. P. Itie, M. Taguchi, C. F. Hague, J. M. Mariot, R. Delaunay, J. P. Kappler, and N. Jaouen, Probing the Transition in Bulk Ce under Pressure: A Direct Investigation by Resonant Inelastic X-ray Scattering, *Phys. Rev. Lett.* **96**, 237403 (2006).
- [5] M. J. Lipp, A. P. Sorini, J. Bradley, B. Maddox, K. T. Moore, H. Cynn, T. P. Devereaux, Y. Xiao, P. Chow, and W. J. Evans, X-ray Emission Spectroscopy of Cerium Across the $\gamma - \alpha$ Volume Collapse Transition, *Phys. Rev. Lett.* **109**, 195705 (2012).
- [6] B. Chen, E. M. Pärshcke, W.-C. Chen, B. Scoggins, B. Li, M. Balasubramanian, S. Heald, J. Zhang, H. Deng, R. Sereika *et al.*, Probing cerium $4f$ states across the volume collapse transition by x-ray Raman scattering, *J. Phys. Chem. Lett.* **10**, 7890 (2019).
- [7] T. Naka, T. Matsumoto, and N. Môri, Magnetic states of $\alpha - \gamma - \text{Ce}$ at high pressure, *Phys. B: Condens. Matter* **205**, 121 (1995).
- [8] J. W. Allen and R. M. Martin, Kondo Volume Collapse and the $\gamma \rightarrow \alpha$ Transition in Cerium, *Phys. Rev. Lett.* **49**, 1106 (1982).
- [9] M. Lavagna, C. Lacroix, and M. Cyrot, Volume collapse in the Kondo lattice, *Phys. Lett. A* **90**, 210 (1982).
- [10] B. Johansson, The $\alpha - \gamma$ transition in cerium is a Mott transition, *Philos. Mag.* **30**, 469 (1974).
- [11] I. Felner and I. Nowik, First-order valence phase transition in cubic $\text{Yb}_x\text{In}_{1-x}\text{Cu}_2$, *Phys. Rev. B* **33**, 617 (1986).
- [12] I. Felner, I. Nowik, D. Vaknin, U. Potzel, J. Moser, G. M. Kalvius, G. Wortmann, G. Schmiester, G. Hilscher, E. Gratz, C. Schmitzer, N. Pillmayr, K. G. Prasad, H. deWaard, and H. Pinto, Ytterbium valence phase transition in $\text{Yb}_x\text{In}_{1-x}\text{Cu}_2$, *Phys. Rev. B* **35**, 6956 (1987).
- [13] K. Kojima, H. Hayashi, A. Minami, Y. Kasamatsu, and T. Hihara, Crystal phases and Yb valence transition in $\text{Yb}_x\text{In}_{1-x}\text{Cu}_2$, *J. Magn. Magn. Mater.* **81**, 267 (1989).
- [14] J. L. Sarrao, A. P. Ramirez, T. W. Darling, F. Freibert, A. Migliori, C. D. Immer, Z. Fisk, and Y. Uwatoko, Thermodynamics of the first-order valence transition in YbInCu_4 , *Phys. Rev. B* **58**, 409 (1998).
- [15] H. Sato, K. Shimada, M. Arita, K. Hiraoka, K. Kojima, Y. Takeda, K. Yoshikawa, M. Sawada, M. Nakatake, H. Namatame, M. Taniguchi, Y. Takata, E. Ikenaga, S. Shin, K. Kobayashi, K. Tamasaku, Y. Nishino, D. Miwa, M. Yabashi, and T. Ishikawa, Valence Transition of YbInCu_4 Observed in Hard X-ray Photoemission Spectra, *Phys. Rev. Lett.* **93**, 246404 (2004).
- [16] S. Tsutsui, K. Sugimoto, R. Tsunoda, Y. Hirose, T. Mito, R. Settai, and M. Mizumaki, First-order structural change accompanied by Yb valence transition in YbInCu_4 , *J. Phys. Soc. Jpn.* **85**, 063602 (2016).
- [17] S. Nesterenko, A. Tursina, M. Pasturel, S. Xhakaza, and A. Strydom, Two polymorphs of a new intermetallic $\text{Ce}_2\text{Rh}_2\text{Ga}$ —

- crystal structure and physical properties, *J. Alloy Comp.* **844**, 155570 (2020).
- [18] N. Kawamura, N. Kanai, H. Hayashi, Y. H. Matsuda, M. Mizumaki, K. Kuga, S. Nakatsuji, and S. Watanabe, Lifetime-broadening-suppressed x-ray absorption spectrum of β -YbAlB₄ deduced from Yb $3d \rightarrow 2p$ resonant x-ray emission spectroscopy, *J. Phys. Soc. Jpn.* **86**, 014711 (2017).
- [19] The crystalline orientation was not specified in the present experiments since we estimated the Ce valence using only the relative intensity among the f^0 , f^1 , and f^2 components in the HERFD-XAS and RXES spectra measured with the fixed experimental set up. In addition, the relative intensity is expected to be almost independent of, or only weakly depend on the crystalline orientation since the Ce L_3 absorption is mainly caused by the $2p_{3/2} - 5d$ transition. Note that the orientation dependence affects only the absolute value of the Ce valence in Fig. 3(b), while does not affect the qualitative temperature dependence.
- [20] H. Yamaoka, I. Jarrige, N. Tsujii, A. Kotani, J.-F. Lin, F. Honda, R. Settai, Y. Onoki, N. Hiraoka, H. Ishii, and K.-D. Tsuei, Pressure and temperature dependencies of the electronic structure of CeIrSi₃ probed by resonant x-ray emission spectroscopy, *J. Phys. Soc. Jpn.* **80**, 124701 (2017).
- [21] Y. Zekko, Y. Yamamoto, H. Yamaoka, F. Tajima, T. Nishioka, F. Strigari, A. Severing, J.-F. Lin, N. Hiraoka, H. Ishii, K.-D. Tsuei, and J. Mizuki, Correlation between the valence state of cerium and the magnetic transition in Ce(Ru_{1-x}Fe_x)₂Al₁₀ studied by resonant x-ray emission spectroscopy, *Phys. Rev. B* **89**, 125108 (2014).
- [22] A. Kotani and Y. Yamaoka, Final-state interaction in the L_3 x-ray absorption spectra of mixed-valence Ce and Yb compounds, *J. Phys. Soc. Jpn.* **84**, 033702 (2015).
- [23] I.-K. Jeong, T. W. Darling, M. J. Graf, Th. Proffen, and R. H. Heffner, Role of the Lattice in the $\gamma \rightarrow \alpha$ Phase Transition of Ce: A High-Pressure Neutron and X-ray Diffraction Study, *Phys. Rev. Lett.* **92**, 105702 (2004).
- [24] D. T. Adroja, B. D. Rainford, J. M. de Teresa, A. del Moral, M. R. Ibarra, and K. S. Knight, First-order valence phase transition in CeNi_{1-x}Co_xSn alloys, *Phys. Rev. B* **52**, 12790 (1995).
- [25] H. Yamaoka, N. Tsujii, K. Yamamoto, H. Oohashi, A. M. Vlaicu, K. Kunitani, K. Uotani, D. Horiguchi, T. Tochio, Y. Ito, and S. Shin, Direct observation of valence transition in CeNi_{1-x}Co_xSn alloys by x-ray and photoelectron spectroscopies, *Phys. Rev. B* **76**, 075130 (2007).
- [26] The as-cast sample with $x = 0.33$ in Ref. [25] exhibit the valence transition around 70 K.
- [27] J.-M. Imer and E. Wuilloud, A simple model calculation for XPS, BIS and EELS $4f$ -excitations in Ce and La compounds, *Z. Phys. B* **66**, 153 (1987).
- [28] O. Gunnarsson and K. Schönhammer, Electron spectroscopies for Ce compounds in the impurity model, *Phys. Rev. B* **28**, 4315 (1983).
- [29] O. Gunnarsson and K. Schönhammer, Double occupancy of the f orbital in the Anderson model for Ce compounds, *Phys. Rev. B* **31**, 4815 (1985).